ACS APPLIED MATERIALS & INTERFACES

Research Article

www.acsami.org

Surface Chemistry of Nanoscale Mineralized Collagen Regulates Periodontal Ligament Stem Cell Fate

Yu Fu, Shuai Liu, Sheng-Jie Cui, Xiao-Xing Kou, Xue-Dong Wang, Xiao-Mo Liu, Yue Sun, Gao-Nan Wang, Yan Liu,* and Yan-Heng Zhou*

Center for Craniofacial Stem Cell Research and Regeneration, Department of Orthodontics, Peking University School and Hospital of Stomatology, National Engineering Laboratory for Digital and Material Technology of Stomatology, Beijing Key Laboratory of Digital Stomatology, Beijing 100081, P. R. China

Supporting Information

ABSTRACT: The interplay between stem cells and their extracellular microenvironment is of critical importance to the stem cell-based therapeutics in regenerative medicine. Mineralized collagen is the main component of bone extracellular matrix, but the effect of interfacial properties of mineralized collagen on subsequent cellular behaviors is unclear. This study examined the role of surface chemistry of nanoscale mineralized collagen on human periodontal ligament stem cell (hPDLSC) fate decisions. The intrafibrillarly mineralized collagen (IMC), fabricated by a biomimetic bottom-up approach, showed a bonelike hierarchy with nanohydroxyapatites (HAs) periodically embedded within fibrils. The infrared spectrum of the IMC showed the presence of phosphate, carbonate, amide I and II bands; and infrared mapping displayed uniform and higher spatial distribution of mineralization in the IMC. However, the distribution of the phosphate group differed far from that of the amide I group in the extrafibrillarly mineralized collagen (EMC), in which flowerlike HA clusters randomly depositing around the surface of the fibrils. Moreover, a large quantity of extrafibrillar HAs covered up the C═O stretch and N−H in-plane bend, resulting in substantial reduction of amide I and II bands. Cell experiments demonstrated that the hPDLSCs seeded on the IMC exhibited a highly branched, osteoblast-like polygonal shape with extended pseudopodia and thick stress fiber formation; while cells on the EMC displayed a spindle shape with less branch points and thin actin fibril formation. Furthermore, the biocompatibility of EMC was much lower than that of IMC. Interestingly, even without osteogenic induction, mRNA levels of major osteogenic differentiation genes were highly expressed in the IMC during cultivation time. These data suggest that the IMC with a similar nanotopography and surface chemistry to natural mineralized collagen directs hPDLSCs toward osteoblast differentiation, providing a promising scaffold in bone tissue regeneration.

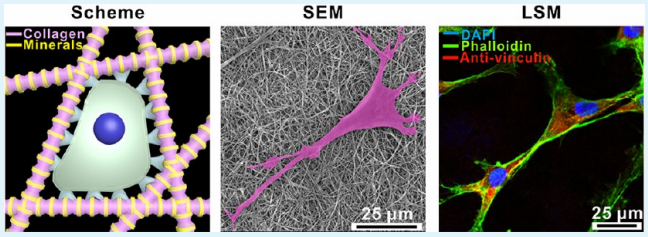

KEYWORDS: *interfacial microenvironment, surface chemistry, intrafibrillar mineralization, cell fate, tissue regeneration*

1. INTRODUCTION

Bone tissue engineering has developed very fast in the past three decades in order to cope with the donor site morbidity and limited availability of autologous bone graft.[1] Tissue-engineering strategies, involving the utilization of stem cells with regenerative capacity and their delivery to the injured sites using biomaterial scaffolds, have been proposed as promising approaches to regenerate lost bone.[2,3] Biomimetic bone graft substitutes are desirable for replacing autologous grafts but difficult for many researchers due to the complexity of bone tissue.[4,5]

It is well-known that both nanotopography and chemical composition of biomaterial could regulate the stem cell fate.[6,7] Bone extracellular matrix (ECM) is mainly composed of type I collagenous fibrils with carbonated hydroxyapatite (HA) nanocrystallites embedded in the gap regions to form intrafibrillar mineralization.[4,5] Mimicking the natural ECM has thus been considered a promising approach in the design of artificial scaffolds for bone regeneration, which favors cellular interactions to the ECM in the initial cell adhesion, morphology, proliferation and further osteogenic differentiation and mineralization.[8] It is well-known that type I collagen has good biocompatibility and resorbability, and high affinity to cells.[9−11] However, the mechanical strength of pure collagen scaffold is too low to bear enough stress and maintain a stable microenvironment for stem cell to regenerate. Thus, mineralization of type I collagen is proposed to improve the physical property. Many research groups have attempted to develop bonelike collagen/HA composites. Nevertheless, the earlier research mainly report on the deposition of HA crystallites around collagen fibrils (i.e., extrafibrillar mineralization) and have only reproduced similar chemical composition rather than nanostructure and surface chemistry of bone ECM.[12,13] As intrafibrillar mineralization has been proven to be a dominant

Received: April 26, 2016
Accepted: June 9, 2016
Published: June 9, 2016

DOI: 10.1021/acsami.6b04951
ACS Appl. Mater. Interfaces 2016, 8, 15958−15966

Table 1. Primer Sequence Used in qRT-PCR

gene	forward primer (5′-3′)	reverse primer (5′-3′)
GAPDH	GGAGCGAGATCCCTCCAAAAT	GGCTGTTGTCATACTTCTCATGG
OPN	GAAGTTTCGCAGACCTGACAT	GTATGCACCATTCAACTCCTCG
COL1A1	GTGCGATGACGTGATCTGTGA	CGGTGGTTTCTTGGTCGGT
BMP-2	ACTACCAGAAACGAGTGGGAA	GCATCTGTTCTCGGAAAACCT

contributor to the biomechanics of natural bone,[14−16] synthesis of mineralized collagen with intrafibrillar HAs is considered as a key factor for mimicking bone ECM and therefore an ideal candidate of bone tissue engineering scaffolds.

Mesenchymal stem cells (MSCs) are widely used in bone tissue engineering, because they can differentiate into multiple lineages, depending on the nature of the environmental signals they receive. Among the dental-derived stem cells, periodontal ligament stem cells (PDLSCs) are of particular interest because they can be efficiently harvested and obtained from discarded biological samples in dental clinics. Furthermore, PDLSCs possess characteristics of putative MSCs and can differentiate into multiple lineages.[17−19] Cytotherapies using PDLSCs have been proved effective to regenerate periodontal tissues in large animal models.[20,21] Additionally, PDLSCs have shown greater capacity for alveolar bone[22] and tendon[23] regeneration than bone marrow MSCs, which are most popular and typical stem cells in bone regeneration. Thus, PDLSCs were attractive candidates in bone tissue engineering, especially for alveolar bone regeneration.

The effective utilization of stem cells in bone regeneration critically depends on our understanding of the intricate interactions between scaffolds and stem cells. The aim of this study was to develop a promising interfacial microenvironment for PDLSCs-based bone regeneration. Mineralized collagen scaffolds with different surface chemistry were fabricated and the in vitro cell responses of PDLSCs to the collagen scaffolds including adhesion, cytoskeletal organization, cell morphology, growth, and osteogenic differentiation were evaluated.

2. MATERIALS AND METHODS

2.1. Preparation of Mineralized Collagen. To reconstitute collagen matrix, 1 mL of type I tropocollagen solution (3.84 mg/mL, M_w 115−235 kDa, Corning) was mixed with 1 mL of 0.1 M acetic acid and 2 mL of a buffer containing 200 mM KCl, 30 mM Na_2HPO_4, and 10 mM KH_2PO_4 at pH 7.[24] Five hundred microliters of the mixture solution was dripped onto a polylysine-coated coverslip of 25 mm diameter and left to gel by incubation at 30 °C for 2−3 days. The fibrillized collagen was cross-linked with 0.3 M 1-ethyl-3(3-(dimethylamino)propyl)-carbodiimide and 0.06 M *N*-hydroxysuccinimide at room temperature, and phosphorylated by 2.5 wt % sodium tripolyphosphate.[25,26] For the preparation of intrafibrillarly mineralized collagen (IMC), the phosphorylated collagen was mineralized for 5 days at 37 °C by a biomimetic bottom-up mineralization approach, in which the mineralization solution was composed of 136.8 mM NaCl, 4.2 mM $NaHCO_3$, 3.0 mM KCl, 1.0 mM $K_2HPO_4{\cdot}3H_2O$, 1.5 mM $MgCl_2{\cdot}6H_2O$, 2.5 mM $CaCl_2$, 0.5 mM Na_2SO_4, 3.08 mM Na_3N, 1 g/15 mL Portland cement (Lehigh Cement Co.) and 0.28 mM poly(acrylic acid) (PAA, M_w 1800, Sigma-Aldrich).[25,26] In the absence of PAA, extrafibrillarly mineralized collagen (EMC) was obtained.

2.2. Scanning Electron Microscopy (SEM). Cell-seeded samples were previously fixed by 2.5% glutaraldehyde. All the samples were dehydrated, critical-point dried, and observed under SEM at 15 kV (Hitachi S-4800, Japan).

2.3. Transmission Electron Microscopy (TEM). TEM was carried out using a JEM-2100F at 120 kV. The samples were deposited on Formvar carbon-coated nickel grids.

2.4. X-ray Diffraction (XRD). XRD was performed to characterize the structure of crystals in different scaffolds using D8 Advance (Bruker, Germany) at 45 kV and 40 mA. To get fine powders, all the samples were thoroughly rinsed with deionized water, critical-point dried, and pulverized in liquid nitrogen. JADE8 software was used to analyze the XRD patterns.

2.5. Fourier Transform Infrared Microspectroscopy (micro-FTIR). LUMOS stand-alone micro-FTIR from Bruker was employed to measure the spatial distribution of different chemical groups in the mineralized collagen. For each sample, interferograms were simultaneously collected from each element of the 64 points (8 × 8 lattice) at a resolution of 1 cm^{-1} using 32 s per point. The imaged sample size was 100 μm × 100 μm. To obtain the spatial distribution of mineral (through integration of the phosphate *v1*, *v3*) and collagen matrix (through integration of the amide I group), the results were plotted as color-coded mapping images. Furthermore, mineral-to-matrix (phosphate/amide I) ratios from 15 infrared spectra were calculated to assess the mineralization level of the collagen scaffolds.[27]

2.6. Cell Isolation and Identification. Human periodontal ligament stem cells (hPDLSCs) were isolated from periodontal ligament tissue of extracted bicuspids from orthodontic patients and cultured with the complete medium (alpha modification of Eagle's medium/10% fetal calf serum/100 U/mL penicillin/100 μg/mL streptomycin) in a humidified atmosphere of 5% CO_2 at 37 °C. The protocol to acquire human tissues was approved by the Ethical Guidelines of Peking University (PKUSSIRB-201311103). To observe the multipotent differentiation ability of hPDLSCs, osteogenicity by alizarin red S staining and adipogenicity by oil red O staining were identified. The specific surface antigens of hPDLSCs such as STRO-1, CD146, and CD44[17] were identified using an Accuri C6 flow cytometer (BD Biosciences) (Figure S1).

For the following studies, cells at passage 4 were seeded on different scaffolds at a density of 2 × 10^5 cells per well. The scaffolds were collected on polylysine-coated coverslips of 25 mm diameter and placed in a 6-well nontreated polystyrene plate with a stainless steel ring to prevent swelling. Before cell seeding, the scaffolds were sterilized under ultraviolet light for 2 h.

2.7. Cell Proliferation Assay. The number of living cells seeded on different scaffolds was estimated using CCK-8 assay (Sigma-Aldrich). The samples, at desired time points (3 and 7 days), were incubated in CCK-8 solution at 37 °C for 2 h. The absorbance was read at 450 nm using a microplate reader (Bio-Rad, Japan). Cell number was positively correlated to the OD value. Each group had six replicates.

2.8. Immunofluorescence Staining. After being cultured for 1 d, hPDLSCs were doubled-stained with Alexa Fluor 488 Phalloidin (F-actin, green) and antivinculin antibody (red). After washing thrice, the cells were mounted with mounting media containing DAPI (blue) for nuclei staining and viewed by a Zeiss laser scanning confocal microscope LSM 710. For each group, 15 cells (three specimens × five cells) were imaged and analyzed. ImageJ was used to measure cell area. The number of branch points was calculated by counting the number of projections from the cell body with a length greater than 5 μm.[28]

2.9. Quantitative Real-Time Polymerase Chain Reaction (qRT-PCR). Cells seeded on different scaffolds were cultured in the complete medium until desired time points (7 and 14 days). Polylysine-coated coverslips without fibrillized collagen were placed in 6-well plates and served as negative controls. Quantitative RT-PCR was applied to examine the expression of osteogenic differentiation gene makers including osteopotin (OPN), alpha-1 type I collagen

DOI: 10.1021/acsami.6b04951
ACS Appl. Mater. Interfaces 2016, 8, 15958−15966

(COL1A1) and bone morphogenetic protein-2 (BMP-2). Glyceraldehyde 3-phosphate dehydrogenase (GAPDH) was used as the housekeeping gene. Total RNA was extracted by Trizol reagent and synthesis of cDNA was performed using SuperScript III One-Step RT-PCR System with Platinum Taq High Fidelity (Invitrogen). Quantitative RT-PCR was performed on a 7900HT Fast Real Time PCR machine (Applied Biosystems) using SYBR Green (Invitrogen Life Technologies). The primers designed by primer premier 5.0 software and commercially synthesized were shown in Table 1.

2.10. Alizarin Red S (ARS) Staining. The amount of ECM secreted by seeded hPDLSCs was analyzed by ARS staining. After cultured in the osteogenic medium (complete medium supplemented with 10^{-7} M dexamethasone, 10 mM β-glycerophosphate and 0.05 mM ascorbic acid 2-phosphates) for 21 days, the cells were fixed using 2% paraformaldehyde for 30 min at room temperature. Half of the samples (N = 6) were stained with 2% alizarin red solution for 20 min at room temperature, and the other half were prepared for SEM examination to observe calcium nodules formed by hPDLSCs. The scaffolds without seeded cells served as controls. After washed for several times with deionized water, the samples were visualized under a light microscope. Then the ARS staining was released from the cell matrix by incubation in 10% cetylpyridinium chloride (Sigma-Aldrich) for 15 min with shaking and the amount of dye released was quantified by spectrophotometer at 562 nm.

2.11. Statistical Analysis. Values were averaged and expressed as mean ± standard deviation. Statistical analysis was performed by one-way ANOVA with Tukey's multiple comparisons test using the SPSS 13.0 program. The differences were considered statistically significant at $\alpha = 0.05$.

3. RESULTS

3.1. Characterization of Mineralized Collagen. The typical micro- and nanostructure of the mineralized collagen was observed by SEM and TEM respectively, as shown in Figure 1. The IMC exhibited a pronounced fibrous (193.1 nm ±22.6 nm) and rough texture with faint cross-banding patterns (Figure 1a), whereas flowerlike HA clusters (ca. 1−4 μm) randomly deposited around the surface of the fibrils (107.7 nm ± 22.4 nm) in the EMC (Figure 1c). The presence of an intrafibrillar HA mineral phase (Ca/P = 1.46) in the IMC was confirmed using energy-dispersive X-ray spectroscopy (EDS) coupled to SEM (Figure S2a). The mineral HA inside the subfibril clusters expanded the width of the fibrils in the IMC compared with pure collagen (COL) (Figure 1e). This observation was further confirmed by TEM, in which nanofibers in the IMC appeared as arrays of electron-dense strands (Figure 1b) according to 67 nm D-period. The TEM analysis verified a high degree of intrafibrillar mineral in the IMC. Selected area electron diffraction (SAED) coupled to TEM was applied to evaluate the mineral phase in the IMC. The SAED pattern showed the crystal planes of nano-HAs as broad arcs for the (002) plane and overlapping arcs for the (112) and (300) planes forming a ring shape. The orientation of the nano-HA (002) reflection was parallel to the *c*-axis of the collagen fibril, matching that of the intrafibrillar mineral in bone. In the EMC, the fibril showed low electron density, with electron-dense HAs depositing around the fibrillar surface (Figure 1d). This observation was consistent with the EDS result, in which the Ca/P molar ratio in the fibril area was 0.4 but 1.98 in the HA area of the EMC (Figure S2b, c). The stained COL showed 67 nm D-period, similar to native collagen (Figure 1f). XRD confirmed the formation of HA crystals in the mineralized collagen (Figure S3). The characteristic peaks of HA, from the (002), (211), (112), and (300) planes, were observed in the EMC and IMC specimens.

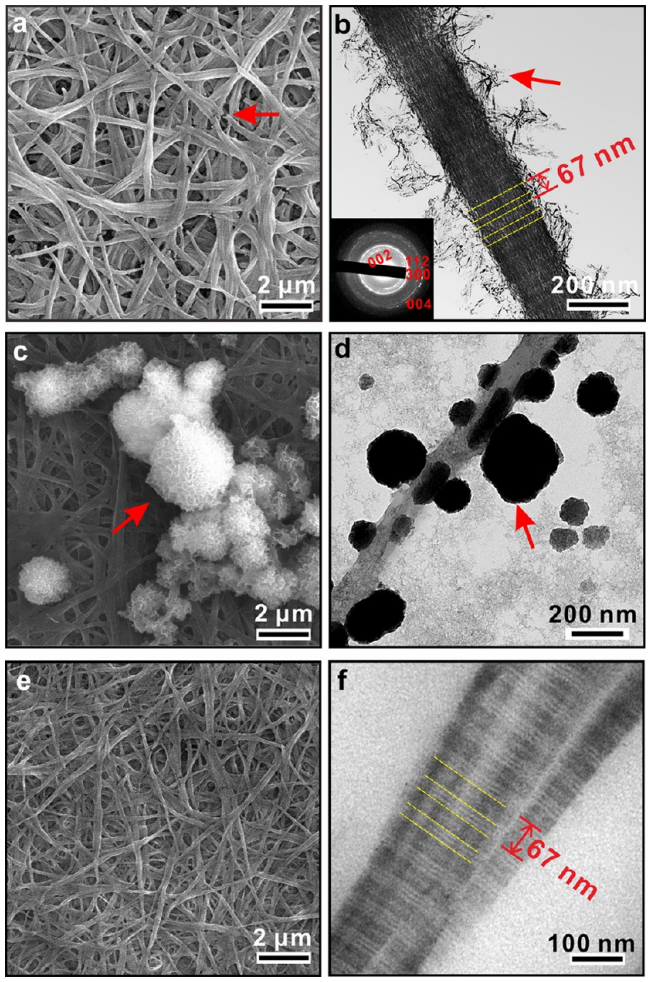

Figure 1. Mineralized collagen fibrils observed by (a, c, e) SEM and (b, d, f) TEM. (a) IMC. Periodic cross-banding patterns could vaguely be observed. Red arrow: brittle fracture. (b) Unstained TEM image of IMC, showing nanofibers with obvious banding patterns. SAED (inset) of the intrafibrillar nanocrystals indicated distinct arc-shaped patterns characteristic of carbonated HAs. Red arrow: extrafibrillar minerals. (c) EMC. Red arrow: flowerlike, spherulitic aggregates. (d) Unstained TEM image of EMC. Red arrow: extrafibrillar HAs with high electron density. (e) COL. (f) Stained TEM image of COL, showing 67 nm D-period.

Micro-FTIR was applied to map the chemical composition and spatial distribution of calcification at micron scale of the mineralized collagen (Figure 2). All spectra displayed typical peaks of collagen: the peak between 1585 and 1720 cm^{-1} was attributed to the C═O stretching vibration (amide I). Absorbance band for amide II (1500−1585 cm^{-1}), arising from angular deformation of N═H bond, was observed in the IMC and COL. Compared with the IMC and COL, the intensity of amide I and amide II bands in the EMC scaffold decreased quite markedly to the extent that the amide II peak nearly disappeared. Typical vibration bands of phosphate (900−1200 cm^{-1}), indicating mineral particles, were identified in both the IMC and EMC scaffolds. Furthermore, the vibration band (855−890 cm^{-1}) of carbonate apatite was also observed in the IMC, resulting in a similar mineral phase to natural bone (Figure 2a). The broad peak between 3000 and 3400 cm^{-1} (OH band) identified in the IMC and COL was related to the absorption of water in the scaffolds.

DOI: 10.1021/acsami.6b04951
ACS Appl. Mater. Interfaces 2016, 8, 15958−15966

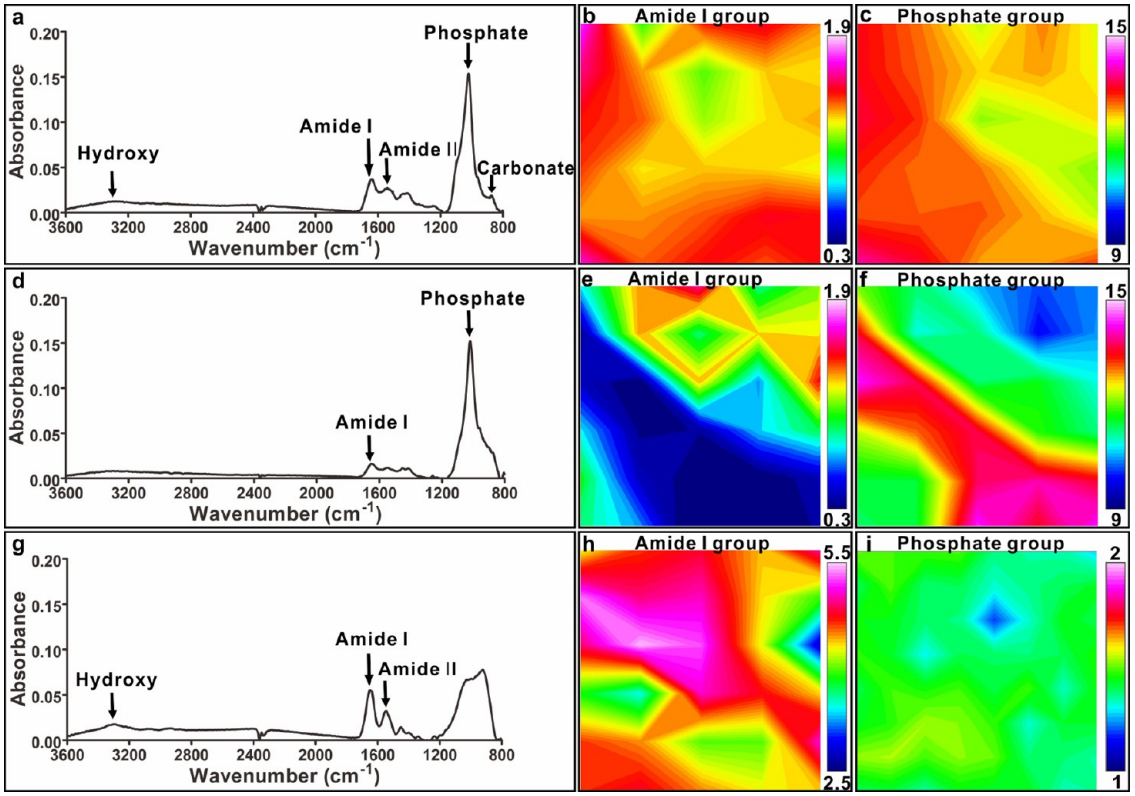

Figure 2. Micro-FTIR spectra and mapping of (a–c) IMC, (d–f) EMC, and (g–i) COL. The color scale indicates the spectral intensity.

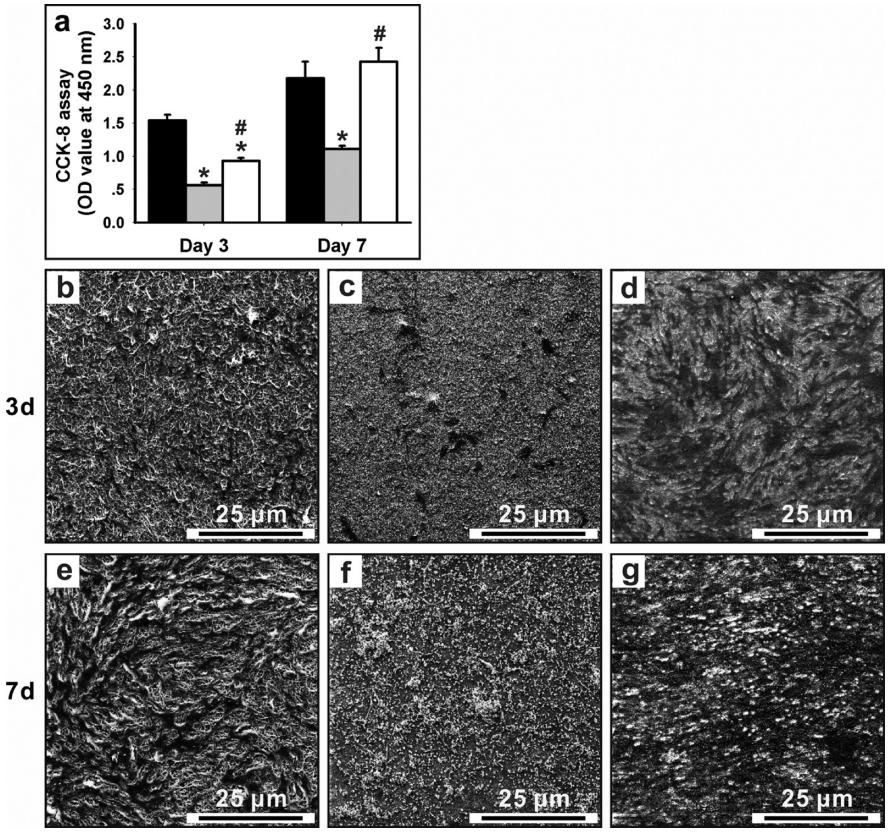

Figure 3. Cell proliferation of hPDLSCs seeded on different scaffolds: (a) CCK-8 assay, (b–g) SEM images of cells seeded on the (b, e) IMC, (c, f) EMC, and (d, g) COL scaffolds on day 3 and day 7. *: $\alpha < 0.05$ versus IMC, #: $\alpha < 0.05$ versus EMC.

DOI: 10.1021/acsami.6b04951
ACS Appl. Mater. Interfaces 2016, 8, 15958–15966

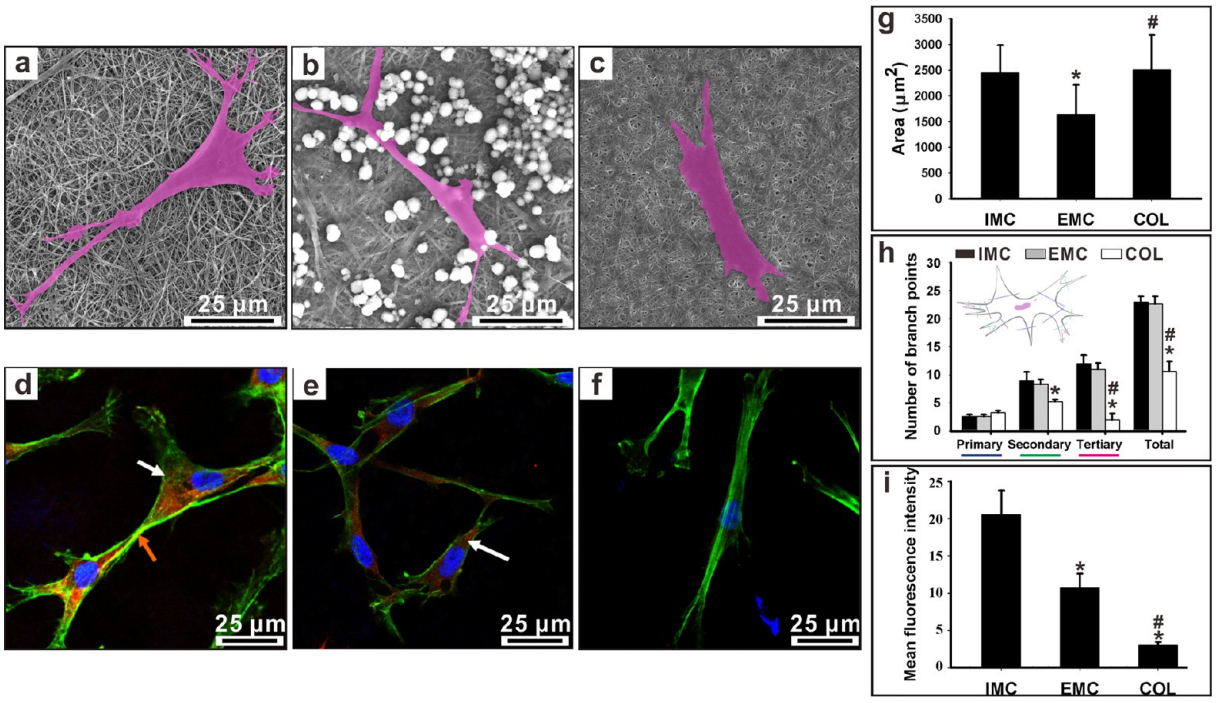

Figure 4. hPDLSC morphology after one-day seeded on different scaffolds tested by (a–c) SEM and (d–f) LSM. (a, d) IMC, (b, e) EMC, (c, f) COL. For the fluorescent microscopic images d–f, triple labeling includes Alexa Fluor 488 Phalloidin (green), antivinculin (red) and DAPI (blue). (g) Cell area, (h) number of branch points, and (i) mean fluorescence intensity of vinculin of hPDLSCs seeded on different scaffolds were quantified (N = 15). *: α < 0.05 versus IMC, #: α < 0.05 versus EMC.

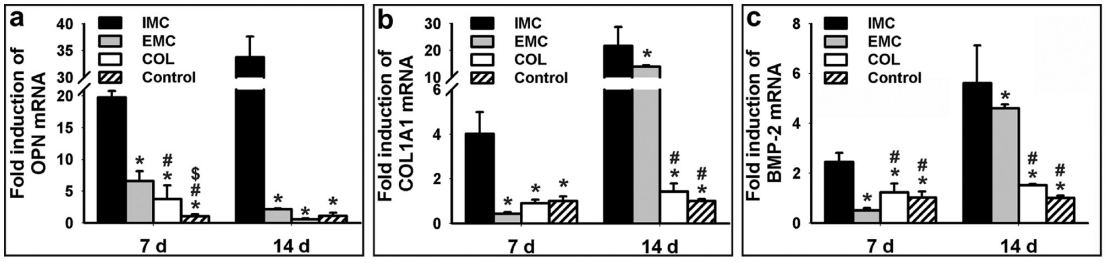

Figure 5. Quantitative RT-PCR measurement of the expression levels of osteogenic differentiation markers: (a) OPN, (b) COL1A1, (c) BMP-2. *: α < 0.05 versus IMC, #: α < 0.05 versus EMC, $: α < 0.05 versus COL.

Scanning images and mapping analysis of the mineralized collagen not only visually confirmed the presence of phosphate within the mineralized collagen but also offered an insight into the mineralization degree and type. The spatial distribution of phosphate and amide I groups was consistent in the IMC (Figure 2b, c), which may suggest the minerals were embedded in the fibrils. However, the distribution of phosphate group differed far from that of amide I group in the EMC (Figure 2e, f), demonstrating that the minerals did not deposited within the fibrils and had little chemical connection with collagen fibrils. These results were consistent with the TEM observations. Moreover, the mineral-to-matrix ratio of IMC (4.3 ± 0.4) was much higher than that of the EMC (1.9 ± 0.3) (Figure S4), indicating a higher mineralization level of the IMC.

3.2. Cell Viability. The isolated hPDLSCs showed multipotent differentiation ability (Figure S1). To investigate the cytocompatibility of scaffold materials, cell attachment and growth rate was measured for hPDLSCs seeded on different scaffolds by CCK-8 and SEM (Figure 3). The CCK-8 assay showed the cell number on different scaffolds increased significantly with the cultivation time (Figure 3a). After 3 days of culture, cell viability was the highest in the IMC group among three groups. However, cells seeded on the IMC scaffold were as many as those on the COL scaffold on day 7. This may indicate that the cells reached confluence and begin to differentiate along an osteogenic lineage, as shown by SEM (Figure 3e, g). Cell viability on the EMC scaffold was the lowest among three groups, indicating that the biocompatibility of this scaffold was much lower than that of IMC and COL. These results were consistent with the SEM observations (Figure 3b–g).

3.3. Cell Morphology and Adhesion. The morphology of hPDLSCs seeded on different scaffolds was examined by SEM (Figure 4a–c) and LSM (Figure 4d–f). After cell seeding for 24 h, hPDLSCs adhered and spread well over all the collagen scaffolds (Figure 4a–c). The cells seeded on the IMC scaffolds exhibited an osteoblast-like polygonal shape with extended pseudopodia, while the cells on the EMC scaffold displayed a spindle shape. This observation was further confirmed by immunofluorescence, where hPDLSCs were double immunostained for F-actin to label the cytoskeletal arrangement and vinculin to label focal adhesion points (FAPs). Among three

DOI: 10.1021/acsami.6b04951
ACS Appl. Mater. Interfaces 2016, 8, 15958–15966

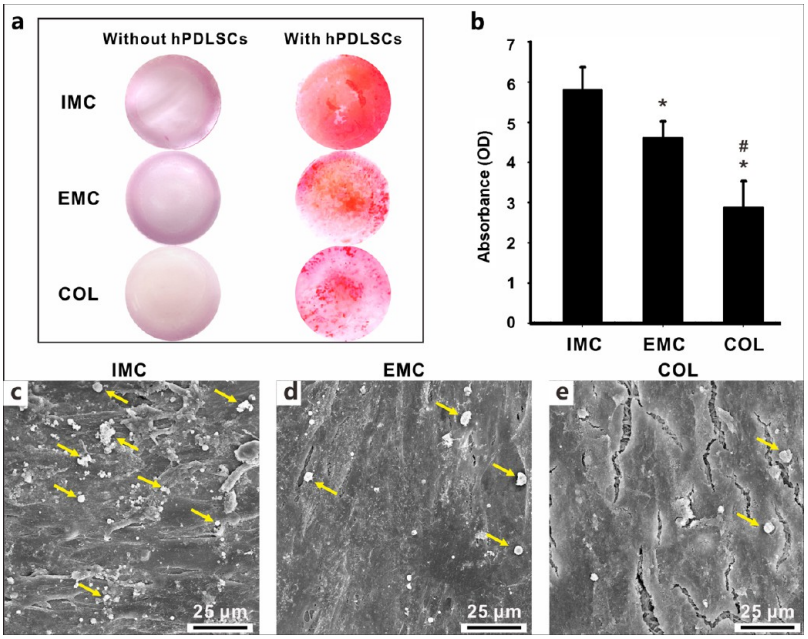

Figure 6. ARS staining and SEM of hPDLSCs seeded on different scaffolds for 21 days: (a) ARS staining, (b) semiquantification of a. (c–e) SEM. Scaffolds without cells served as controls. SEM showed that the hPDLSCs seeded on the IMC secreted more mineralized particles (yellow arrows) than those on the EMC and COL. *: $\alpha < 0.05$ versus IMC, #: $\alpha < 0.05$ versus EMC.

scaffolds, concentrated intertwined stress fibers (arrows) could only be formed at the cellular periphery of hPDLSCs seeded on the IMC scaffold. In addition, immunostaining of vinculin was detected in the hPDLSCs seeded on the IMC and EMC scaffolds but could be barely detected on the COL scaffold (Figure 4d–f). From the quantitative data, hPDLSCs seeded on the IMC scaffold had more cell area and branch points than those on the EMC scaffold (Figure 4g, h). More importantly, the highest density of FAPs was observed on the surface of the IMC scaffold among the three groups (Figure 4i).

3.4. Osteogenic Differentiation. To evaluate the effects of different scaffolds on hPDLSC differentiation, we evaluated the expression levels of osteogenic markers (Figure 5) and in vitro calcification (Figure 6). Quantitative RT-PCR showed that mRNA levels of OPN, COL1A1, and BMP-2 in hPDLSCs from the IMC group were up-regulated more than twice compared with the control group during the cultivation time. Cells grown on the EMC scaffold expressed more than twice as much OPN while COL1A1 and BMP-2 were down-regulated compared with the control group on day 7. An opposite tendency was observed on day 14. Higher expression of COL1A1 and BMP-2 was detected in the EMC group, whereas the mRNA level of OPN was not significantly affected by the EMC scaffold with respect to the control group. Among four groups, hPDLSCs seeded on the IMC scaffold exhibited the highest expression levels of those genes during the cultivation time, indicating that the IMC scaffold showed the biggest potential to induce osteogenic differentiation of hPDLSCs.

The mineralization of ECM on different scaffolds was illustrated by ARS staining, in which calcium deposits produced by hPDLSCs were stained with orange-red spots. The scaffolds without seeded hPDLSCs served as controls in order to exclude the interference of intra- and extra-fibrillar minerals in the scaffolds (Figure 6a). Compared with the COL and EMC scaffolds, the IMC scaffold promoted calcium deposition in hPDLSCs after 21 days of culture in the osteogenic medium by ARS staining (Figure 6a, b). Meanwhile, SEM showed that the hPDLSCs seeded on the IMC secreted more mineralized particles (Figure 6c, yellow arrow) than those on the EMC and COL (Figure 6d, e, yellow arrow).

4. DISCUSSION

In this study, two types of mineralized collagen were fabricated and exhibited different surface topography and chemistry. The IMC showed a pronounced fibrous topography with no evidence of surface deposits of mineral clusters, as seen in the EMC. This may be attributed to the important role of PAA as a mimic of noncollagenous proteins in stabilizing the crystallizing solution and producing liquid like amorphous calcium phosphate nanoclusters.[25,26] The phosphorylated collagen fibrils template the hierarchical deposition of amorphous nanoculsters in the gap regions, followed by HA crystallization to form a periodic arrangement of mineral,[25,26] which closely resembles the fundamental nanostructure of natural bone.[4,5] In the absence of an anionic polymer, collagen mineralization involves heterogeneous HA nucleation on the surface of the collagen fibrils, which is drastically different from the bone structure.

The recently developed micro-FTIR, which offers a unique insight at the molecular scale to monitor the structural changes of biosamples,[29] was applied to determine the microstructural details on chemical composition and spatial distribution of calcification of the scaffolds. The infrared spectrum of the IMC showed the presence of phosphate, carbonate (from carbonate substitution for hydroxyl and phosphate groups in HA), amide I and II bands, which is quite similar to that of natural bone.[30] Compared with the COL, the intensity of amide I and II bands in the IMC only decreased a little, whereas that in the EMC reduced substantially (Figure 2). This may be because a large quantity of HAs deposited around the collagen fibril surface and covered up the C═O stretch (amide I) and N–H in-plane bend (amide II). Previous study has demonstrated that calcium phosphate crystals could block the one-dimensional vibration C═O stretch and the two-dimensional vibration N–H in-plane

DOI: 10.1021/acsami.6b04951
ACS Appl. Mater. Interfaces 2016, 8, 15958–15966

bend during collagen mineralization.[31] Besides, the peak intensity of OH band in the EMC was much lower than that in the IMC and COL, indicating that the calcium ions may chelate with hydroxyl group at the surface of collagen fibrils and then grow into microscale particles.

It has been proven that collagen/HA matrix could direct MSCs into osteogenic differentiation.[32,33] The different chemical combination patterns between HAs and collagen in the IMC and EMC have already affected the nanostructure and surface chemistry of scaffolds. Whether this difference could influence stem cell fate was further tested. We have proven that the IMC could promote the proliferation of hPDLSCs compared with the EMC and pure COL as illustrated by CCK-8 and SEM results. The shape, size and crystallinity of HA particles could affect the cell activity and proliferative ability and induce inflammation.[34−36] Microscale HA with high crystallinity has higher cytotoxity. The EMC had microscale HA particles deposited on the surface of collagen fibrils, which may have slight cytotoxity and result in the smallest cell number even after hPDLSCs cultured on the EMC for 7 days. Therefore, the biocompatibility of IMC was much better than EMC and similar to pure COL, which is commonly recognized as a biocompatible biomaterial.

The different interfacial properties of the ECM including surface nanotopography and chemistry could cause a significant difference in the cell adhesion and morphology.[37−40] The cells seeded on the IMC exhibited a highly branched, osteoblast-like polygonal shape with extended pseudopodia and thick stress fiber formation; whereas those on the EMC scaffold displayed a spindle shape with less branch points and thin actin fibril formation. Flat cells (lack of 3D organization) with least branch points were found in the COL. The above differences in cell morphology might be attributed to cytoskeleton rearrangement. This assumption was confirmed by immunofluorescence, where hPDLSCs were immunostained for F-actin. Among three scaffolds, concentrated intertwined stress fibers could only be formed at the cellular periphery of hPDLSCs seeded on the IMC. Previous studies have demonstrated that thick actin stress fibers could facilitate intracellular signal transduction and then osteogenic differentiation of MSCs.[41,42] Thus, it is possible that hPDLSCs seeded on IMC would be more like to differentiate into osteoblasts.

It is signals coming from extracellular microenvironment that could induce the morphological and cytoskeletal changes in cells seeded on scaffolds. The connection between ECM and cell is established on FAPs, which are large macromolecular assemblies. To see whether there are differences in FAPs expression among hPDLSCs seed on different scaffolds, immunostaining of vinculin, an intracellular part of FAPs, was detected. The addition of inorganic components into ECM could enhance the vinculin expression, compared to pure collagen.[32] In the present study, the vinculin staining was more abundant in the IMC and EMC than that in the COL. It is $\alpha 2\beta 1$ integrin, a transmembrane protein of FAPs, through which cell binds to type I collagen. Metal ions and glutamate from type I collagen play a critical role in ligand binding for $\alpha 2\beta 1$ integrin.[43] The FTIR results revealed that the amide I band was exposed in larger quantity at the surface of IMC than that of EMC. This may facilitate the direct bond between metal ions and carboxylate oxygens from collagen glutamate (represented by amide I) and further activate $\alpha 2\beta 1$ integrin to promote the vinculin expression of hPDLSCs (Figure 7). Taken together, the quantitative data showed that the highest

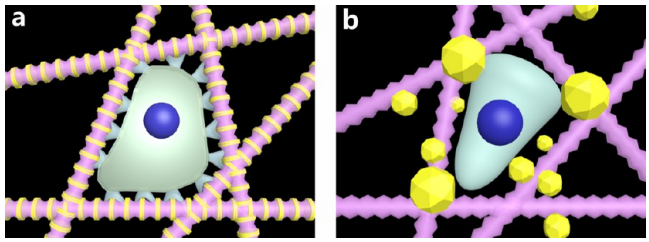

Figure 7. Scheme of cell-scaffold interactions. (a) Morphology of hPDLSC seeded on the IMC. Large amounts of exposed collagen component promoted binding of hPDLSCs to the IMC. (b) Morphology of hPDLSC seeded on the EMC. Microscale HAs covered the surface of collagen and blocked the interactions between hPDLSCs and collagen. Pink represents collagen fibrils and yellow represents mineral HAs.

density of FAPs was observed in the IMC group among three groups. The reorganization of actin filaments might derive from the higher density of FAPs shown on the IMC, as focal adhesion plays an important role in linking the ECM on the outside to the actin cytoskeleton on the inside at the cell-matrix interface.[40] Then the actin cytoskeleton organization may further affect the cell morphology so that hPDLSCs seeded on the IMC scaffold had more cell area and branch points than those on the EMC.

The highly branched polygonal morphology, actin cytoskeleton reorganization and high expression of FAPs have been shown to be closely related to the osteogenic differentiation of stem cells.[28,44] The osteogenic activity of the hPDLSCs was further evaluated by measuring their mRNA expression levels of bone-related markers including OPN, COL1A1, and BMP-2. OPN, a secreted glycophosphoprotein, is believed to play a crucial role in regulating HA crystal growth in bone formation.[45] Previous studies have proven that the OPN expression is stimulated when osteoblastic cells are seeded on type I collagen fibrils.[46] As the most abundant extracellular protein in bone, COLI provides the structural framework for bone formation. BMP-2 is an important signaling protein in the process of bone repair.[47] The stimulating effect of the IMC on osteogenic differentiation of hPDLSCs was further confirmed by ARS staining. We have proven that the IMC had nanotopographic and surface chemical characteristics similar to natural bone. However, how these differences interfered with the hPDLSC cell fate remains unclear. On one hand, from the perspective of topography, the osteoinductive effect of the IMC might ascribe to its fibrous and rough nanotopography.[48] The flowerlike shape, microscale size, and high crystallinity of HA particles in the EMC result in lower cell viability and further osteogenic differentiation ability.[34,35] On the other hand, the differences in osteogenic effect among the IMC, EMC, and COL might be attributed to the chemical interactions between minerals and collagen. Previous studies have suggested type I collagen could induce the osteoblastic differentiation of bone marrow cells through collagen-$\alpha 2\beta 1$ integrin interaction.[49] As mentioned above, the IMC may enhance the activity of $\alpha 2\beta 1$ integrin, which could in turn promote the osteogenic differentiation of hPDLSCs through $\alpha 2\beta 1$ integrin-FAK-ERK pathway.[50]

5. CONCLUSION

In sum, the mineralized collagen scaffolds exhibit different nanotopography and chemical distribution. The surface

DOI: 10.1021/acsami.6b04951
ACS Appl. Mater. Interfaces 2016, 8, 15958−15966

chemistry of mineralized collagen regulates the hPDLSC fate, including adhesion, cytoskeletal organization, cell morphology, growth and osteogenic differentiation. The intrafibrillar mineralization of collagen provides a niche more like in vivo bone ECM and shows promising potential for bone tissue regeneration. Further research is needed to demonstrate the mechanism of fate changes induced by nanosurface properties and also the in vivo bone regeneration potential of the IMC.

■ ASSOCIATED CONTENT

Supporting Information

The Supporting Information is available free of charge on the ACS Publications website at DOI: 10.1021/acsami.6b04951.

Figure S1, c multipotent differentiation potential and surface marker expressions of hPDLSCs; Figure S2, EDX plots with corresponding SEM images; Figure S3, X-ray diffraction spectra of COL, EMC, and IMC specimens; Figure S4, phosphate/amide I ratio of IMC and EMC scaffolds (PDF)

■ AUTHOR INFORMATION

Corresponding Authors

*E-mail: orthoyan@bjmu.edu.cn. Tel.: +86 10 82195975. Fax: +86 10 82195536.

*E-mail: yanhengzhou@gmail.com. Tel.: +86 10 82195728. Fax: +86 10 82195536.

Author Contributions

Y.F. contributed to conception, design, data acquisition, analysis and interpretation, drafted the manuscript; Y.L. and Y.-H.Z. contributed to conception, design, data analysis and interpretation and critically revised the manuscript; X.-X.K., S.L., and S.-J.C. contributed to data analysis and interpretation and critically revised the manuscript; X.-D.W. and X.-M.L., contributed to design and data interpretation, critically revised the manuscript; Y.S. and G.-N.W. contributed to data analysis and critically revised the manuscript. All authors gave final approval and agreed to be accountable for all aspects of the work.

Notes

The authors declare no competing financial interest.

■ ACKNOWLEDGMENTS

This work was supported by National Natural Science Foundation of China (81571815) and Beijing Municipal Natural Science Foundation (7152156). The authors declare no potential conflicts of interest with respect to the authorship and/or publication of this article.

■ REFERENCES

(1) Ahlmann, E.; Patzakis, M.; Roidis, N.; Shepherd, L.; Holtom, P. Comparison of Anterior and Posterior Iliac Crest Bone Grafts in terms of Harvest-Site Morbidity and Functional Outcomes. *J. Bone Joint Surg. Am.* **2002**, *84*, 716−720.

(2) Chen, F. M.; Sun, H. H.; Lu, H.; Yu, Q. Stem Cell-Delivery Therapeutics for Periodontal Tissue Regeneration. *Biomaterials* **2012**, *33*, 6320−6344.

(3) Honda, M. J.; Imaizumi, M.; Tsuchiya, S.; Morsczeck, C. Dental Follicle Stem Cells and Tissue Engineering. *J. Oral Sci.* **2010**, *52*, 541−552.

(4) Katz, E. P.; Li, S. T. Structure and Function of Bone Collagen Fibrils. *J. Mol. Biol.* **1973**, *80*, 1−15.

(5) Lees, S.; Prostak, K. The Locus of Mineral Crystallites in Bone. *Connect. Tissue Res.* **1988**, *18*, 41−54.

(6) Griffin, M. F.; Butler, P. E.; Seifalian, A. M.; Kalaskar, D. M. Control of Stem Cell Fate by Engineering Their Micro and Nanoenvironment. *World J. Stem Cells* **2015**, *7*, 37−50.

(7) Watt, F. M.; Hogan, B. L. Out of Eden: Stem Cells and Their Niches. *Science* **2000**, *287*, 1427−1430.

(8) Ma, P. X. Biomimetic Materials for Tissue Engineering. *Adv. Drug Delivery Rev.* **2008**, *60*, 184−198.

(9) Mauney, J.; Volloch, V. Progression of Human Bone Marrow Stromal Cells into Both Osteogenic and Adipogenic Lineages is Differentially Regulated by Structural Conformation of Collagen I Matrix via Distinct Signaling Pathways. *Matrix Biol.* **2009**, *28*, 239−250.

(10) Xia, Z.; Yu, X.; Jiang, X.; Brody, H. D.; Rowe, D. W.; Wei, M. Fabrication and Characterization of Biomimetic Collagen-Apatite Scaffolds with Tunable Structures for Bone Tissue Engineering. *Acta Biomater.* **2013**, *9*, 7308−7319.

(11) Holzwarth, J. M.; Ma, P. X. Biomimetic Nanofibrous Scaffolds for Bone Tissue Engineering. *Biomaterials* **2011**, *32*, 9622−9629.

(12) Zhang, W.; Liao, S. S.; Cui, F. Z. Hierarchical Self-assembly of Nano-Fibrils in Mineralized Collagen. *Chem. Mater.* **2003**, *15*, 3221−3226.

(13) Cui, F.; Li, Y.; Ge, J. Self-assembly of Mineralized Collagen Composites. *Mater. Sci. Eng., R* **2007**, *57*, 1−27.

(14) Cointry, G. R.; Capozza, R. F.; Chiappe, M. A.; Feldman, S.; Meta, M. D.; Daniele, S. M.; Fracalossi, N. M.; Reina, P.; Ferretti, J. L. Novel Experimental Effects on Bone Material Properties and the Pre- and Postyield Behavior of Bones may be Independent of Bone Mineralization. *J. Bone Miner. Metab.* **2005**, *23*, 30−35.

(15) Balooch, M.; Habelitz, S.; Kinney, J. H.; Marshall, S. J.; Marshall, G. W. Mechanical Properties of Mineralized Collagen Fibrils as Influenced by Demineralization. *J. Struct. Biol.* **2008**, *162*, 404−410.

(16) Weiner, S.; Traub, W.; Wagner, H. D. Lamellar Bone: Structure-Function Relations. *J. Struct. Biol.* **1999**, *126*, 241−255.

(17) Seo, B. M.; Miura, M.; Gronthos, S.; Bartold, P. M.; Batouli, S.; Brahim, J.; Young, M.; Robey, P. G.; Wang, C. Y.; Shi, S. Investigation of Multipotent Postnatal Stem Cells from Human Periodontal Ligament. *Lancet* **2004**, *364*, 149−155.

(18) Silverio, K. G.; Rodrigues, T. L.; Coletta, R. D.; Benevides, L.; Da Silva, J. S.; Casati, M. Z.; Sallum, E. A.; Nociti, F. H., Jr. Mesenchymal Stem Cell Properties of Periodontal Ligament Cells from Deciduous and Permanent Teeth. *J. Periodontol.* **2010**, *81*, 1207−1215.

(19) Iwata, T.; Yamato, M.; Zhang, Z.; Mukobata, S.; Washio, K.; Ando, T.; Feijen, J.; Okano, T.; Ishikawa, I. Validation of Human Periodontal Ligament-Derived Cells as a Reliable Source for Cytotherapeutic Use. *J. Clin. Periodontol.* **2010**, *37*, 1088−1099.

(20) Liu, Y.; Zheng, Y.; Ding, G.; Fang, D.; Zhang, C.; Bartold, P. M.; Gronthos, S.; Shi, S.; Wang, S. Periodontal Ligament Stem Cell-Mediated Treatment for Periodontitis in Miniature Swine. *Stem Cells* **2008**, *26*, 1065−1073.

(21) Iwata, T.; Yamato, M.; Tsuchioka, H.; Takagi, R.; Mukobata, S.; Washio, K.; Okano, T.; Ishikawa, I. Periodontal Regeneration with Multi-Layered Periodontal Ligament-Derived Cell Sheets in a Canine Model. *Biomaterials* **2009**, *30*, 2716−2723.

(22) Tsumanuma, Y.; Iwata, T.; Washio, K.; Yoshida, T.; Yamada, A.; Takagi, R.; Ohno, T.; Lin, K.; Yamato, M.; Ishikawa, I.; Okano, T.; Izumi, Y. Comparison of Different Tissue-Derived Stem Cell Sheets for Periodontal Regeneration in a Canine 1-Wall Defect Model. *Biomaterials* **2011**, *32*, 5819−5825.

(23) Moshaverinia, A.; Xu, X.; Chen, C.; Ansari, S.; Zadeh, H. H.; Snead, M. L.; Shi, S. Application of Stem Cells Derived from the Periodontal Ligament or Gingival Tissue Sources for Tendon Tissue Regeneration. *Biomaterials* **2014**, *35*, 2642−2650.

(24) Leow, W. W.; Hwang, W. Epitaxially Guided Assembly of Collagen Layers on Mica Surfaces. *Langmuir* **2011**, *27*, 10907−10913.

(25) Liu, Y.; Li, N.; Qi, Y. P.; Dai, L.; Bryan, T. E.; Mao, J.; Pashley, D. H.; Tay, F. R. Intrafibrillar Collagen Mineralization Produced by Biomimetic Hierarchical Nanoapatite Assembly. *Adv. Mater.* **2011**, *23*, 975−980.

DOI: 10.1021/acsami.6b04951
ACS Appl. Mater. Interfaces 2016, 8, 15958−15966

(26) Liu, Y.; Kim, Y. K.; Dai, L.; Li, N.; Khan, S. O.; Pashley, D. H.; Tay, F. R. Hierarchical and Non-Hierarchical Mineralization of Collagen. *Biomaterials* **2011**, *32*, 1291−1300.
(27) Deegan, A. J.; Cinque, G.; Wehbe, K.; Konduru, S.; Yang, Y. Tracking Calcification in Tissue-Engineered Bone Using Synchrotron Micro-FTIR and SEM. *Anal. Bioanal. Chem.* **2015**, *407*, 1097−1105.
(28) Kumar, G.; Tison, C. K.; Chatterjee, K.; Pine, P. S.; McDaniel, J. H.; Salit, M. L.; Young, M. F.; Simon, C. G., Jr. The Determination of Stem Cell Fate by 3D Scaffold Structures through the Control of Cell Shape. *Biomaterials* **2011**, *32*, 9188−9196.
(29) Petibois, C.; Piccinini, M.; Guidi, M. C.; Marcelli, A. Facing the Challenge of Biosample Imaging by FTIR with a Synchrotron Radiation Source. *J. Synchrotron Radiat.* **2010**, *17*, 1−11.
(30) Boskey, A.; Pleshko Camacho, N. FT-IR Imaging of Native and Tissue-Engineered Bone and Cartilage. *Biomaterials* **2007**, *28*, 2465−2478.
(31) Zhang, W.; Huang, Z. L.; Liao, S. S.; Cui, F. Z. Nucleation Sites of Calcium Phosphate Crystals during Collagen Mineralization. *J. Am. Ceram. Soc.* **2003**, *86*, 1052−1054.
(32) He, J.; Jiang, B.; Dai, Y.; Hao, J.; Zhou, Z.; Tian, Z.; Wu, F.; Gu, Z. Regulation of the Osteoblastic and Chondrocytic Differentiation of Stem Cells by the Extracellular Matrix and Subsequent Bone Formation Modes. *Biomaterials* **2013**, *34*, 6580−6588.
(33) He, J.; Meng, G.; Yao, R.; Jiang, B.; Wu, Y.; Wu, F. The Essential Role of Inorganic Substrate in the Migration and Osteoblastic Differentiation of Mesenchymal Stem Cells. *J. Mech. Behav Biomed. Mater.* **2016**, *59*, 353−365.
(34) Grandjean-Laquerriere, A.; Laquerriere, P.; Guenounou, M.; Laurent-Maquin, D.; Phillips, T. M. Importance of the Surface Area Ratio on Cytokines Production by Human Monocytes in vitro Induced by Various Hydroxyapatite Particles. *Biomaterials* **2005**, *26*, 2361−2369.
(35) Shi, Z.; Huang, X.; Cai, Y.; Tang, R.; Yang, D. Size Effect of Hydroxyapatite Nanoparticles on Proliferation and Apoptosis of Osteoblast-Like Cells. *Acta Biomater.* **2009**, *5*, 338−345.
(36) Zhao, Y.; Zhang, Y.; Zhao, Y.; Hou, S.; Chu, P. K. Synthesis and Cellular Biocompatibility of Two Nanophase Hydroxyapatite with Different Ca/P Ratio. *J. Nanosci. Nanotechnol.* **2011**, *11*, 11069−11073.
(37) Perez, R. A.; Ginebra, M. P. Injectable Collagen/A-Tricalcium Phosphate Cement: Collagen-Mineral Phase Interactions and Cell Response. *J. Mater. Sci.: Mater. Med.* **2013**, *24*, 381−393.
(38) Baslé, M. F.; Grizon, F.; Pascaretti, C.; Lesourd, M.; Chappard, D. Shape and Orientation of Osteoblast-Like Cells (Saos-2) are Influenced by Collagen Fibers in Xenogenic Bone Biomaterial. *J. Biomed. Mater. Res.* **1998**, *40*, 350−357.
(39) Ayala, R.; Zhang, C.; Yang, D.; Hwang, Y.; Aung, A.; Shroff, S. S.; Arce, F. T.; Lal, R.; Arya, G.; Varghese, S. Engineering the Cell-Material Interface for Controlling Stem Cell Adhesion, Migration, and Differentiation. *Biomaterials* **2011**, *32*, 3700−3711.
(40) Yim, E. K.; Darling, E. M.; Kulangara, K.; Guilak, F.; Leong, K. W. Nanotopography-induced Changes in Focal Adhesions, Cytoskeletal Organization, and Mechanical Properties of Human Mesenchymal Stem Cells. *Biomaterials* **2010**, *31*, 1299−1306.
(41) Müller, P.; Langenbach, A.; Kaminski, A.; Rychly, J. Modulating the Actin Cytoskeleton Affects Mechanically Induced Signal Transduction and Differentiation in Mesenchymal Stem Cells. *PLoS One* **2013**, *8*, e71283.
(42) Mathieu, P. S.; Loboa, E. G. Cytoskeletal and Focal Adhesion Influences on Mesenchymal Stem Cell Shape, Mechanical Properties, and Differentiation Down Osteogenic, Adipogenic, and Chondrogenic Pathways. *Tissue Eng., Part B* **2012**, *18*, 436−444.
(43) Emsley, J.; Knight, C. G.; Farndale, R. W.; Barnes, M. J.; Liddington, R. C. Structural Basis of Collagen Recognition by Integrin Alpha2beta1. *Cell* **2000**, *101*, 47−56.
(44) Uzer, G.; Pongkitwitoon, S.; Ete Chan, M.; Judex, S. Vibration Induced Osteogenic Commitment of Mesenchymal Stem Cells is Enhanced by Cytoskeletal Remodeling but Not Fluid Shear. *J. Biomech.* **2013**, *46*, 2296−2302.
(45) Wada, T.; McKee, M. D.; Steitz, S.; Giachelli, C. M. Calcification of Vascular Smooth Muscle Cell Cultures: Inhibition by Osteopontin. *Circ. Res.* **1999**, *84*, 166−178.
(46) Carvalho, R. S.; Kostenuik, P. J.; Salih, E.; Bumann, A.; Gerstenfeld, L. C. Selective Adhesion of Osteoblastic Cells to Different Integrin Ligands Induces Osteopontin Gene Expression. *Matrix Biol.* **2003**, *22*, 241−249.
(47) Nishii, N.; Arai, M.; Yanai, N.; Togari, A.; Nakabayashi, T. Effect of Bone Morphogenetic Protein-2 (BMP-2) or Troglitazone, as an Inducer of Osteogenic Cells or Adipocytes, on Differentiation of a Bone Marrow Mesenchymal Progenitor Cell Line Established from Temperature-Sensitive (Ts) Simian Virus (SV) 40 T-Antigen Gene Transgenic Mice. *Biol. Pharm. Bull.* **2009**, *32*, 10−17.
(48) Dalby, M. J.; Gadegaard, N.; Curtis, A. S. G.; Oreffo, R. O. C. Nanotopographical Control of Human Osteoprogenitor Differentiation. *Curr. Stem Cell Res. Ther.* **2007**, *2*, 129−138.
(49) Mizuno, M.; Fujisawa, R.; Kuboki, Y. Type I Collagen-induced Osteoblastic Differentiation of Bone-Marrow Cells Mediated by Collagen-Alpha2beta1 Integrin Interaction. *J. Cell. Physiol.* **2000**, *184*, 207−213.
(50) Leyva-Leyva, M.; López-Díaz, A.; Barrera, L.; Camacho-Morales, A.; Hernandez-Aguilar, F.; Carrillo-Casas, E. M.; Arriaga-Pizano, L.; Calderón-Pérez, J.; García-Álvarez, J.; Orozco-Hoyuela, G.; Piña-Barba, C.; Rojas-Martínez, A.; Romero-Díaz, V.; Lara-Arias, J.; Rivera-Bolaños, N.; López-Camarillo, C.; Moncada-Saucedo, N.; Galván-Delos Santos, A.; Meza-Urzúa, F.; Villarreal-Gómez, L.; Fuentes-Mera, L. Differential Expression of Adhesion-Related Proteins and MAPK Pathways Lead to Suitable Osteoblast Differentiation of Human Mesenchymal Stem Cells Subpopulations. *Stem Cells Dev.* **2015**, *24*, 2577−2590.

DOI: 10.1021/acsami.6b04951
ACS Appl. Mater. Interfaces 2016, 8, 15958−15966